On-line Calibration of Lossless Current Sensing

Yang Zhang, Regan Zane, Dragan Maksimovic
Colorado Power Electronics Center
ECE Department, University of Colorado
Boulder, CO 80309-0425
{yyzhang, zane, maksimov}@colorado.edu

Aleksandar Prodic
ECE Department, University of Toronto
10 King's College Road, Toronto, Canada, M5S 3G4
prodic@power.ele.utoronto.ca

***Abstract*—In this paper, we describe a lossless current sensing method with on-line calibration where an auxiliary switch and a precision sense resistor are connected in parallel with a main power switch to achieve accuracy comparable to the sense resistor method, together with the advantage of essentially no additional power loss. The proposed current-sensing circuit and the calibration methods are particularly well suited for digital controller implementations where the required control and calibration functions can be easily accomplished. Experimental results with a digitally controlled 1.5 V, 15 A synchronous buck converter demonstrate functionality of the on-line calibration approach, showing a significant improvement in accuracy over voltage sensing across the power MOSFET on-resistance.**

Keywords - current sensing; calibration; switching power supplies

I. INTRODUCTION

Switching power converters require current sensing for a combination of reasons, including: (a) current-mode control implementation, (b) current sharing among paralleled modules, (c) output voltage positioning (as in voltage regulator modules (VRM)), and (d) over-load protection. In high-frequency DC-DC switching converters, the most commonly used current-sensing methods are summarized in Table I [1-5].

TABLE I. SUMMARY OF CURRENT-SENSING METHODS.

Method name in this paper	Current-sensing method
RS	Sensing the voltage across a series sense resistor R_s
RON	Sensing the voltage across the on resistance R_{on} of a power MOSFET
RL	Sensing and filtering the voltage across an inductor
RW	Sensing the voltage across the PCB wire trace having R_w resistance
SFET	Using a power MOSFET with built-in current-sensing mirror ("SenseFet")
CT	Using a current transformer in series with a power switch

This work was supported by Artesyn Technologies through Colorado Power Electronics Center.

The current-sensing methods differ in how they address the trade-offs among the opposing requirements resulting from the following key considerations:

1. Power loss due to the sensor
2. Accuracy with respect to parameter tolerances and temperature variations
3. Operating range and linearity
4. Bandwidth
5. Sensitivity to switching noise
6. Complexity and cost of implementation

The method of choice usually depends on the specific application requirements. For example, the RS method is often preferred in power-factor-correction or off-line applications because of its accuracy and simplicity. However, in low-voltage, high-current point-of-load applications (such as VRMs), the RON, RL or RW methods are the most commonly applied because they do not induce any additional power losses, and do not require any additional components. But, these "lossless" current-sensing methods have relatively poor accuracy due to tolerances and temperature variations of the sensing resistance (R_{on}, R_L, or R_w). Furthermore, because of the desire to maintain high efficiencies even as the regulated output voltages are decreasing (approaching 1 V or less), the voltage drop allowed across the sensing resistance becomes lower, which further adversely affects the current-sensing accuracy and sensitivity to noise.

In this paper, we propose a lossless current sensing method with on-line calibration where an auxiliary switch Q_a and a sense resistor R_s are connected in parallel with a main power switch Q as shown in Fig. 1, to achieve *combined* advantages of the accurate RS method and the lossless sensing techniques. In normal switching cycles, the main switch Q is turned on to conduct the current i_{sw}. Any of the lossless current sensing

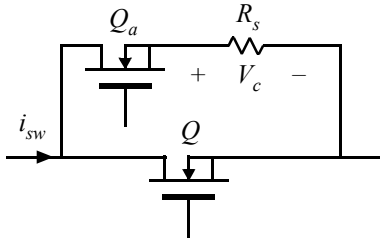

Figure 1. Current-sensing calibration circuit consisting of an auxiliary switch Q_a and a precision sensing resistor R_s in parallel with a main power switch Q. The auxiliary switch is turned on infrequently, only to perform on-line calibration of a lossless current sensing method.

methods (such as RON, RL, or RW sensing), or sensorless current estimation [6], can be performed continuously. In a calibration cycle, which is performed only occasionally, the main switch Q is kept off, while the auxiliary switch Q_a is turned on to conduct the current i_{sw}. The voltage V_c across the precision current-sense resistor R_s is sensed and used to calibrate the lossless current sensing or the sensorless current estimator. Since the calibration cycle is performed only infrequently, e.g. once in every 1000 normal cycles, the auxiliary switch can be rated at a lower current, and the additional loss associated with the auxiliary circuit is negligible. Depending on the application, the auxiliary circuit can be used in parallel with any of the power switches, and the proposed approach can be applied in conjunction with any of the lossless current-sensing methods, or in conjunction with a sensorless current estimation.

In this paper we focus on application of the on-line calibrated current sensing in low-voltage point-of-load dc power supplies or VRMs based on a synchronous buck converter. In this application, it is convenient to add the auxiliary current-sensing circuit across the synchronous rectifier.

The paper is organized as follows. Application of the proposed current-sensing method in a low-voltage synchronous buck converter is described in Section II, together with several calibration techniques that can be implemented in the proposed method. It is noted that the method is particularly well suited for digital controller implementation where the required control and calibration functions can be easily accomplished. Section III presents an experimental test circuit used to validate the proposed approach. Experimental results that demonstrate significant improvement in accuracy over the RON method without penalty in the converter efficiency are summarized in Sections IV and V.

II. Current-Sensing Circuit with On-Line Calibration

Our approach is based on combining the RS method as a calibration stage together with any of the lossless current sensing approaches. In this section, we describe a combination of the RS and RON methods, as shown in Fig. 2 for a synchronous buck converter with current sensing across the synchronous rectifier. During normal operation, the converter runs in the RON mode with Q_2 on over the time interval $(1-D)T_s$, while Q_3 is off. In the normal cycle, the sensed voltage V_s is used to measure the inductor current as:

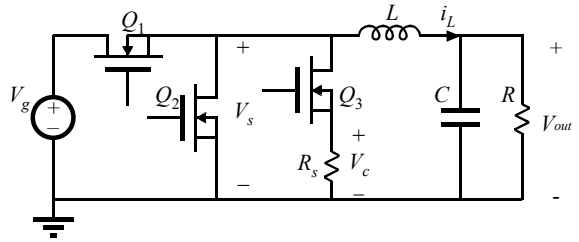

Figure 2. Synchronous Buck converter with current-sensing circuit for on-line calibration

$$I_{sense} = \frac{-V_s}{R_{on}}, \tag{1}$$

where R_{on} is initially estimated from the MOSFET datasheet (or some other best estimate).

The RON approach provides the benefits of no additional components or power loss, but results in poor accuracy due to the component tolerances and sensitivity to temperature. We propose to gain the accuracy benefits of a sense resistor while maintaining the RON benefit of no additional power loss by occasionally switching to the auxiliary MOSFET Q_3 for calibration, while the main synchronous rectifier Q_2 is kept off. In a calibration cycle, the inductor current flows through Q_3 and the accurate sense resistor R_s, resulting in a more precise current measurement:

$$I_{calib} = \frac{-V_c}{R_s}. \tag{2}$$

The calibration cycle is performed infrequently as required for accurate calibration, allowing a relatively small device Q_3 to be used. Here, we describe three approaches for calibrating R_{on} based on the configuration of Fig. 2.

A. Basic calibration of current sensing

The most straightforward application of (2) is to assume that the inductor current is not affected by the calibration cycle, resulting in a calibrated value of the on resistance given by:

$$R_{on\_calib} = R_s \frac{V_s}{V_c}. \tag{3}$$

Then in following normal cycles, this R_{on_calib} is used in (1) instead of the nominal R_{on} to obtain a current sensing accuracy comparable to the RS method. Calibration can be performed infrequently, e.g. every thousands of cycles, to maintain the benefit of lossless RON sensing, while keeping track of slow changes in operating conditions, such as temperature. Note that the approach can calibrate out the effects of temperature variations without sensing the temperature itself, and can also remove other uncertainties, such as component tolerances and aging. The accuracy of the method depends on the sense resistor R_s, and the assumption that the inductor current is not disturbed during the calibration cycles.

In the circuit of Fig. 2, although the auxiliary switch Q_3 can have a lower current rating compared to the main synchronous rectifier Q_2, the combined on-resistance of Q_3 and R_s must be low enough so that the body diode of Q_2 is not turned on during calibration cycles. Another practical concern is that a calibration cycle should be performed only when the circuit is operating in steady state, but not in transients.

B. Estimation of the error induced in i_L during calibration

The calibration cycle itself can induce errors in the inductor current due to an increase in the voltage drop across Q_3 and R_s compared to the voltage drop across the main synchronous rectifier Q_2. This creates a larger inductor voltage during calibration, resulting in an increased current slope as shown in

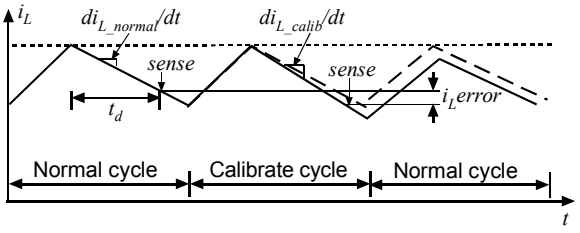

Figure 3. Error induced in the inductor current during calibration. cycles

Fig. 3. The induced error can be particularly large in converters (such as VRMs) with low output voltages and low inductance values. This error can be estimated and cancelled assuming that the inductance value L and the time delay t_d for sampling are known:

$$i_{L\_error} = t_d \cdot \left(\frac{(-V_{s\_calib}) - (-V_{s\_normal})}{L} \right),$$
$$R_{on\_calib} = R_c \cdot \frac{V_{s\_normal}}{V_c} \cdot \frac{1}{1 + \frac{i_{L\_error} \cdot R_c}{-V_c}}, \quad (4)$$

where V_{s_normal} and V_{s_calib} are the voltages at V_s in Fig. 2 during normal and calibration cycles, respectively.

The additional costs of implementing (4) over (3) include sensing V_s and V_c simultaneously during calibration cycles, and the added computational requirements in (4). The approach is well suited for applications with digital control, where the additional processing requirements can be provided at minimal cost.

The primary drawback of (4) is the dependence on the inductance value, whose tolerance and variation may not fall within the requirements for precision current limiting, precision current sharing, or other applications that may require accurate absolute current sensing. Additional accuracy can be gained by using multiple samples during the calibration cycle to measure the inductor current slope and actively estimate the inductance value. When even greater accuracy is required, the active cancellation approach of the following section can be used.

C. *Active cancellation of error induced in i_L*

The next improvement is to actively remove the error induced by the calibration cycles from the measurement by adjusting the duty cycle. This approach can also be used to actively remove any other perturbations in the waveforms resulting from the calibration cycles.

One active cancellation option is a 3-cycle calibration sequence. The first cycle is a preparation cycle (Q_3 on, Q_2 off), the second is a compensation cycle (Q_2 on, Q_3 off) and the third cycle is the actual sensing cycle (Q_3 on, Q_2 off), as shown in Fig. 4.

In the first cycle, V_{s_calib} is sensed to gain the knowledge of i_{L_slope}. The purpose of the compensation in the second cycle is to force the current at the sensing point of the 3rd cycle to reach the same value that the inductor current has in normal cycles at

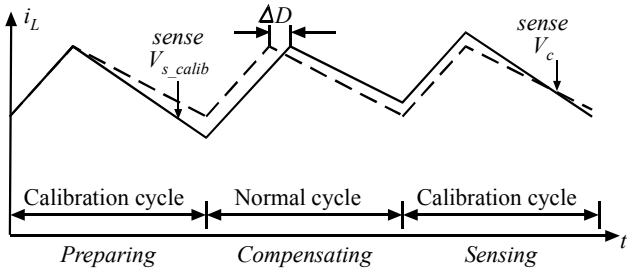

Figure 4. Active cancellation of the error induced in i_L

the time the sampling is performed. The duty cycle is increased by ΔD in the 2nd cycle to compensate for the current error induced in the 1st and the 3rd calibration cycles:

$$\Delta D = \frac{((-V_{s\_calib}) - (V_{s\_normal}))}{V_g} \cdot \left(\frac{t_d}{T_s} + (1 - D) \right), \quad (5)$$

resulting in a measured V_c in the 3rd cycle that can be used directly in (3) to calibrate R_{on}. One key benefit of (5) is that it does not depend on the inductance value, thus having the potential for facilitating very accurate lossless current sensing.

In Sections III, IV and V, an experimental circuit and experimental results are presented for the calibration methods based on (3) and (4).

III. Experimental Test Circuit

An experimental test circuit was built to validate the proposed current sensing and calibration approaches. The test circuit is shown in Fig. 5.

The power stage is a synchronous buck converter operating at 100 kHz switching frequency. The input voltage can be 5 V or 12 V. The output voltage can be 1.2 V, 1.5 V, or 1.8 V. The load current is between 0 A and 15 A. Two synchronous-buck MOSFET drivers (TPS2838) are used to drive the main control switch Q_1, the main synchronous rectifier Q_2, and the auxiliary

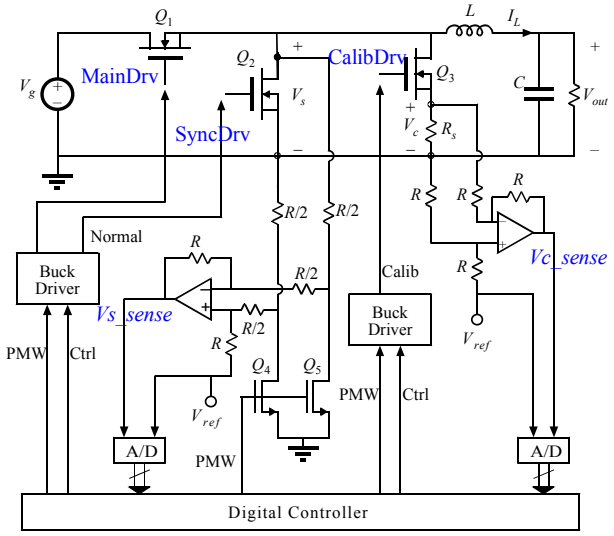

Figure 5. Experimental test circuit for the on-line calibrated current sensing method in a synchronous Buck converter.

calibration rectifier Q_3. The nominal on resistance for Q_2 is 2.9 mΩ (two Si4888DY MOSFETs in parallel). The nominal inductance value is $L = 3.0$ µH and the output capacitance is $C = 750$ µF. The sense resistor is $R_s = 10$ mΩ.

An FPGA-based digital controller is used to generate the gate-drive signals and to control the current-sampling A/D converters.

Two operational amplifiers (OPA350) and the surrounding circuitry perform differential sensing of V_s and V_c, as well as level shifting of the sensed voltages by V_{ref}. The outputs of the operational amplifiers V_{s_sense} and V_{c_sense} satisfy:

$$V_{s\_sense} = V_{ref} - V_s, \qquad V_{c\_sense} = V_{ref} - V_c. \tag{6}$$

The small MOSFET switches Q_4 and Q_5 are used to protect the V_s sensing operational amplifier from the high voltage (5 V or 12 V) when the main control MOSFET Q_1 is on. Compared with sensing V_s and V_c directly, sensing V_{s_sense} and V_{c_sense} has the following benefits:

- V_{s_sense} has much smaller pulsating component than V_s;
- V_{s_sense} and V_{c_sense} have an adjustable common-mode voltage V_{ref}, which can be used to fit the sensed analog signals into the common mode input range of the analog to digital converters;
- RC filters can be added to filter out high-frequency noise from V_s and V_c;
- Differential amplifiers reject the common mode noise at the ground of the power stage.

IV. Experimental Results

For the experimental results reported in this paper, the synchronous buck converter operates at 100 kHz switching frequency, with 12 V input voltage and 1.5 V output voltage. Four load cases have been tested from no load to full load. In order to test and display alternating normal and calibration cycles easily, the circuit is controlled to have one calibration cycle every three normal cycles. A conversion start signal is also generated for A/D converters to sample and hold V_s and V_c with approximately the same time delay in each cycle.

Fig. 6 shows the three gate-drive signals and the inductor current waveform when the circuit is operating at full load. The average value of the inductor current is 15.7 A (10 A/div). MainDrv, SyncDrv and CalibDrv are the gate drive signals for the main control switch Q_1, the main synchronous rectifier Q_2, and the auxiliary calibration rectifier Q_3, respectively.

Fig. 7 shows the voltages V_s, V_c, the inductor current i_L and the conversion start signal at full load. The large pulsating component can be observed in V_s, which goes to approximately 12 V when the main control switch is on, and close to zero when one of the synchronous rectifiers (main or calibration) is on. In normal cycles, when the main synchronous rectifier is on, the voltage V_s across the synchronous rectifier is negative, but very close to zero, because of the very low on resistance of Q_2. Since Q_3 is off during normal cycles, V_c is zero. During

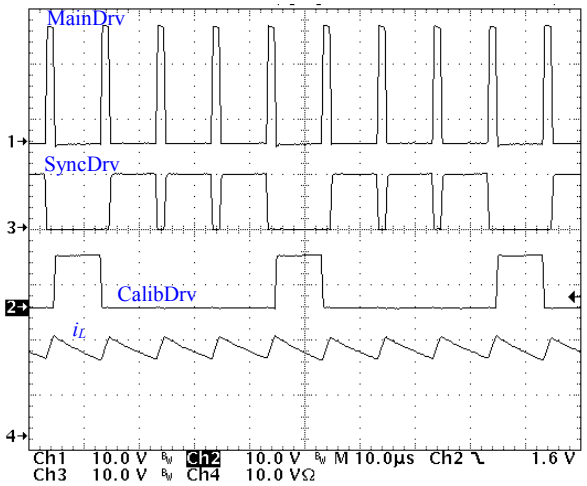

Figure 6. Top-to-bottom: the gate drive signal for the main control switch Q_1; gate drive signal for the main synchronous rectifier Q_2; gate drive signal for the auxiliary calibration rectifier Q_3 and the inductor current at maximum load (15 A).

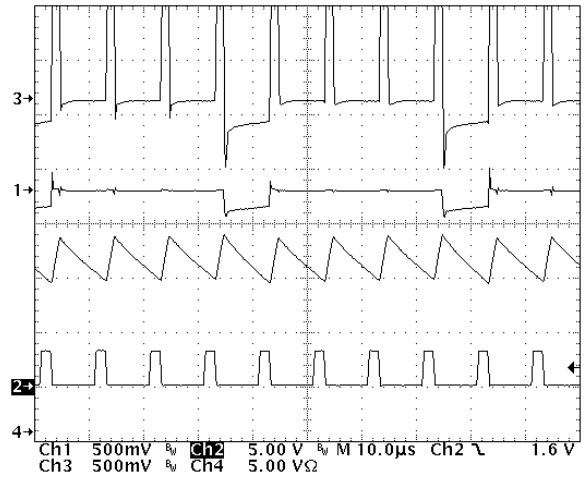

Figure 7. Top-to-bottom: V_s (Ch. 3), V_c (Ch. 1), inductor current (Ch. 4) and conversion start signal (Ch. 2) at maximum load (15 A).

calibration cycles, Q_3 is on and Q_2 is off. As a result, V_c has a more visible negative value because of the larger voltage drop across the sense resistor R_s. The voltage V_s across Q_3 and R_s is also larger than in normal cycles. A small disturbance produced by the calibration cycles can be observed in the inductor current waveform.

Fig. 8 shows the voltage waveforms V_{s_sense}, and V_{c_sense} at the outputs of the differential sensing amplifiers, together with the inductor current and the conversion start signals at full load (15 A). Compared to the V_s waveform of Fig. 7, V_{s_sense} has a much smaller pulsating component. During DT_s, when the main control switch Q_1 is on, V_{s_sense} is somewhat lower than V_{ref} because of the voltage drops across the on-resistances of the small protection switches Q_4 and Q_5.

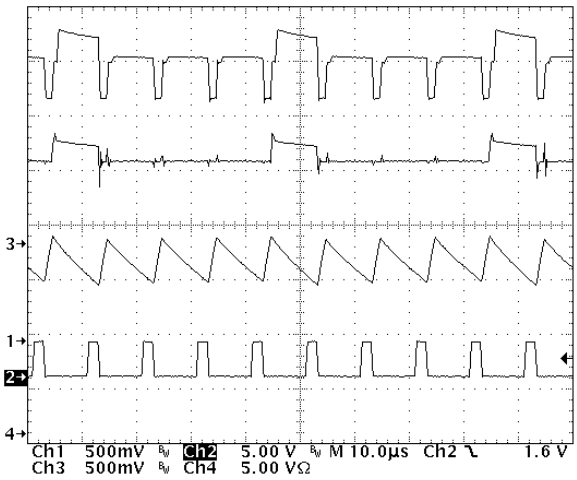

Figure 8. Top-to-bottom: V_{s_sense} (Ch.3), V_{c_sense} (Ch.1) , the inductor current (Ch.4), and the conversion start signal (Ch.2) at maximum load (15 A).

A. *Experimental verification of the basic calibration of current sensing*

The sensing delay t_d is measured between the time a synchronous rectifier (main or calibration) is turned on and the time the rising edge of the conversion start signal samples the sensed signal. In the experiments reported in this section, the sensing delay is t_d = 6.7 µs. At full load, in normal cycles, we have the following result for V_s sensing:

$$-V_{s\_normal} = V_{s\_sense} - V_{ref} = 52mV \tag{7}$$

If only the RON sensing method is used, without calibration, the nominal value of the Q_2 on resistance yields the following estimate for the sensed current:

$$I_{sense} = \frac{-V_s}{R_{on}} = \frac{52mV}{2.9m\Omega} = 17.9A \tag{8}$$

In the calibration cycles, we sense V_{c_sense} at the rising edge of the conversion start signal to obtain:

$$-V_c = V_{c\_sense} - V_{ref} = 143mV \tag{9}$$

Using (2) and (3) we get the calibrated value for the sensed current:

$$I_{calib} = \frac{-V_c}{R_s} = \frac{143mV}{10m\Omega} = 14.3A \tag{10}$$

The current values obtained in (8) and (10) can be compared to the actual current I_{actual} = 14.6 A. The sensing (8) based on the nominal on resistance value results in 23% error, while the calibrated value (10) is off by only 2.1%.

Following the same procedure, four load cases have been tested: 15 A, 9 A, 4.5 A and no load. The results are shown in Table II. We can see that the calibrated sensed current has significant improvement in accuracy compared to the current sensed based on the nominal R_{on} of the main synchronous rectifier.

TABLE II. EXPERIMENTAL RESULTS FOR BASIC CALIBRATION

Load (W)	**23.6**	**13.3**	**6.75**	**0**
Actual current (A)	14.6	8.1	3.8	-0.68
$-V_{s\_normal}$ (mV)	52	32	16	-4
Error (%) in I_{sense} (current sensed by RON method only)	**22.8**	**36.2**	**45.2**	**102.8**
$-V_c$ (mV)	143	80	37	7.3
Error (%) in I_{calib} (current sensed by on-line calibrated RON method)	**-2.1**	**-1.2**	**-2.6**	**7.3**

The basic calibration method can have very good performance when the inductance value and the output voltage in the converter circuit are not too low, so that the inductor current error induced during calibration cycles can be ignored. If this is not the case, the more accurate calibration methods of Sections II.B or II.C can be employed.

B. *Experimental verification of the estimation of the error induced in i_L*

By adding the complexity of sampling V_s and V_c simultaneously during calibration cycles and performing the computations of (4), the improved on-line calibrated sensing results of Table III were obtained. The results are shown for two cases: (a) current errors were compensated based on the nominal inductance value, L = 3.0 µH, and (b) current errors were compensated based on the active estimation of the inductance value. The results based on the nominal L show an improvement over the results of Table II at maximum load. Additional accuracy was achieved by sampling V_c at two points during the calibration cycle to actively estimate the inductance value for use in (4).

Additional accuracy may be required in applications such as VRMs where very low inductance values are used with high currents, which may lead to larger errors than those shown in Tables II and III. In such applications, the method of Section II.C can be used to cancel out the dependence on precise knowledge of the inductance.

TABLE III. EXPERIMENTAL RESLUTS FOR ON-LINE CALIBRATED CURRENT SENSING WITH INDUCTOR CURRENT ERROR COMPENSATION

Load (W)	**23.6**	**13.3**	**6.75**	**0**
$L_{nominal}$ (µH)	3.0	3.0	3.0	3.0
(a) Error (%) in I_{calib} with nominal L used in (4)	**0.93**	**1.6**	**0.49**	**9.6**
$L_{estimated}$ (µH)	3.3	3.9	4.5	5.1
(b) Error (%) in I_{calib} with estimated L used in (4)	**0.66**	**0.96**	**-0.45**	**8.5**

V. LOAD CURRENT SENSING APPLICATION EXAMPLE

In this section, we consider an application example where the purpose of current sensing is to estimate the average inductor current, which is equal to the load current in the synchronous buck converter. To accomplish this, we choose the sensing delay t_d to be equal to one half of the synchronous rectifier on time,

$$t_d = (1-D)\cdot T_s / 2 . \quad (11)$$

Fig. 9 shows the waveforms V_{s_sense}, V_{c_sense}, i_L and conversion start signal at full load, when the sensing point is in the middle of the synchronous rectifier on time. The first cycle shown is a normal cycle and the second cycle is a calibration cycle. V_s and V_c are sensed with the same delay t_d = 4.3 µs.

The current-sensing results for the four load cases are shown in Table IV. I_{calib} is the current sensed by the on-line calibrated RON method using (2) and (3). It can be observed that the proposed method allows accurate load current sensing.

Fig. 10 shows the V_s, V_c, i_L and conversion start signal when the converter is operated at zero load. V_c and V_s waveforms go from negative to positive when the inductor current i_L goes from positive to negative. When the sensing point is in the middle of the synchronous rectifier on time, the sensed voltages V_s and V_c are nearly zero, resulting in a large relative error in the calibration process. Options to avoid large errors at light load include reverting back to the RON method until larger currents are detected, or changing the delay t_d to avoid the zero crossing of the inductor current.

VI. CONCLUSIONS

This paper describes a lossless current sensing method with on-line calibration where an auxiliary switch and a precision sense resistor are connected in parallel with a main power switch to achieve accuracy comparable to the sense resistor method, together with the advantage of essentially no additional power loss. The proposed current-sensing circuit and the calibration methods are particularly well suited for digital controller implementations where the required control and calibration functions can be easily accomplished. Experimental results with a digitally controlled 12 V-to-1.5 V synchronous buck converter operating at 100 kHz switching frequency demonstrate functionality of the proposed sensing and calibration, and a significant improvement in accuracy over voltage sensing across the power MOSFET on-resistance.

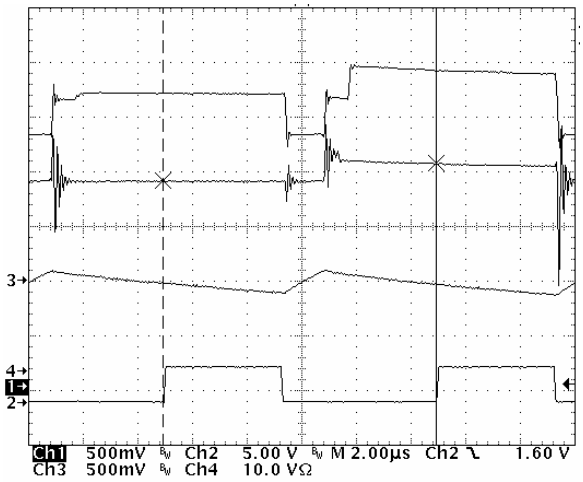

Figure 9. Sensing and calibrating the average inductor current. Top-to-bottom: V_{s_sense} (Ch. 3), V_{c_sense} (Ch. 1), i_L (Ch. 4) and conversion start signal (Ch. 2) at full load (15 A). The vertical cursors are shown at the current sensing points in the normal (first) and calibration (second) cycles.

TABLE IV. EXPERIMENTAL RESLUTS FOR THE LOAD CURRENT SENSING APPLICATION EXAMPLE

Actual current (A)	**15.8**	**9.0**	**4.55**	**0.0**
Error (%) in I_{sense} (current sensed by RON method only)	30.9	38.7	53.9	/
Error (%) in I_{calib} (current sensed by on-line calibrated RON method)	**-1.1**	**-0.7**	**0.1**	/

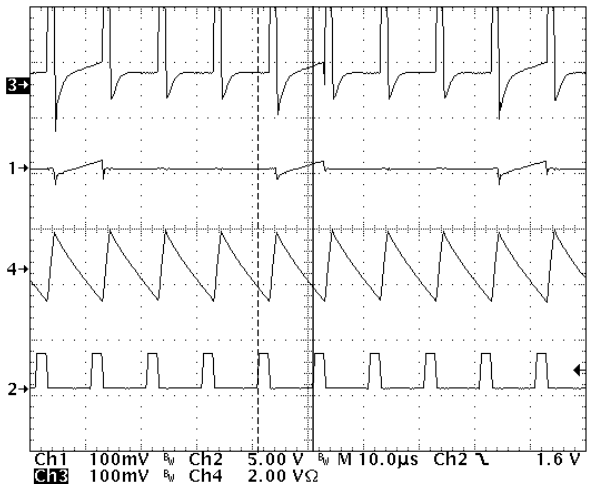

Figure 10. Top-to-bottom: V_s (Ch. 3), V_c (Ch. 1), the inductor current (Ch. 4) and conversion start signal (Ch. 2) at zero load (0 A).

REFERENCES

[1] H.P. Forghani-zadeh, G.A. Rincón-Mora, "Current-sensing techniques for DC-DC converters," The 45th IEEE Midwest Symposium on Circuits and Systems, 2002, pp. 577 –580.

[2] E. Dallago, M. Passoni, G. Sassone, "Lossless current sensing in low-voltage high-current DC/DC modular supplies," IEEE Transactions on Industrial Electronics, Vol.47, No.6, Dec 2000, pp.1249 –1252.

[3] D. Grant, R. Williams, "Current Sensing MOSFETs for Protection and Control," IEE Colloquium on Measurement Techniques for Power Electronics, 1992, pp. 8/1-8/5.

[4] Current-sensing power MOSFETs, ON Semiconductor application note, AND8093/D, July 2002, Rev.5.

[5] Ron Lenk, "Optimum current sensing techniques in CPU converters," Fairchild Application Bulletin AB-20.GI.

[6] P.Midya; M.Greuel, P.T.Krein, "Sensorless current mode control - an observer-based technique for DC-DC converters," IEEE Transactions on Power Electronics, Vol.16, No.4 , Jul 2001, pp.522 –526.